Demountable reinforced concrete slabs using dry connection

Demountable reinforced concrete slabs using dry connection

Hanady Almahmood[1*], Ashraf Ashour[2], Diogo Figueira[3], Gurkan Yildirim[4], Alper Aldemir[5] and Mustafa Sahmaran[6]

[1] Assistant professor, Civil Engineering Department, Applied Science Private University, Amman, Jordan; Tel: 00962-790409743; Email: h_almahmood@asu.edu.jo

[1] Postdoctoral research assistant, Civil Engineering Department, Faculty of Engineering and Informatics, University of Bradford, Bradford, West Yorkshire, BD7 1DP, UK Email address: h.a.a.a.almahmood@ bradford.ac.uk

[2] Professor of Structural Engineering, Civil Engineering Department, Faculty of Engineering and Informatics, University of Bradford, Bradford, West Yorkshire, BD7 1DP, UK Email address: A.F.Ashour@bradford.ac.uk

[3] Post-doctoral Research Assistant, Faculty of Engineering & Informatics, University of Bradford, Bradford BD7 1DP, UK. E-mail: diogo_silva@hotmail.com.

[4] Marie Skłodowska-Curie Individual Fellow, Civil Engineering Department, Faculty of Engineering and Informatics, University of Bradford, Bradford, West Yorkshire, BD7 1DP, UK Email address: gyildirim@bradford.ac.uk

[4] Associate Professor, Department of Civil Engineering, Hacettepe University, Ankara, Turkey. E-mail: gurkanyildirim@hacettepe.edu.tr

[5] Associate Professor, Department of Civil Engineering, Hacettepe University, Ankara, Turkey. E-mail: alperaldemir@hacettepe.edu.tr

[6] Professor, Department of Civil Engineering, Hacettepe University, Ankara, Turkey. E-mail: sahmaran@hacettepe.edu.tr

* Corresponding author
Dr Hanady Almahmood,
Email: h.a.a.almahmood@gmail.com
Phone: +962 0790409743

Abstract

This paper presents an experimental investigation of a new dry connection for reinforced concrete slab elements. Seven full-scale slabs were tested; one slab was monolithic as control specimens, while the other six were assembled using top and bottom steel plates joined by high tensile steel bolts. Two scenarios were proposed for the connection, a simple bolted connection, and a connection with a shear key. The parameters studied were the use of stirrups at the connection section, the step size of the shear key as well as the bolt diameter and number. The test results showed that using a shear key at the assembled section in demountable slabs is more efficient than the simple bolted connection, providing higher flexural stiffness, load capacity, and less deflection. However, increasing the shear key step size improved the flexural performance of the demountable slabs. In addition, adding stirrups to the assembled section enhanced the flexural stiffness and the total load capacity of the demountable slabs. Furthermore, the predictions for the moment capacity and deflection demountable slabs have reasonably good agreement with the experimental results but require additional calibrated data from experiments to be generalized.
Keywords: Dry connections; Deconstruction; Demountable; slabs and plates; Concrete structures.

1. Introduction

Design for deconstruction (DfD) is a developing concept, contributing to the sustainability of construction industry by allowing the reuse of structural elements from disassembled buildings. The main advantage of this concept is the reduction in pollution caused by the demolishment of buildings at the end of their life. In addition, the demountable system means that the structural parts can be connected and disconnected in a short period compared to cast-in-situ construction, leading to more efficient use of resources and a significant reduction in demolition waste and cost [1, 2]. However, the concept of demounting is not possible for cast in situ or precast reinforced concrete (RC) structures, depending on the utilized assembly method. For example, the demounting process becomes impossible for prefabricated RC structures with semi-dry connections where grout or even steel welding between the connected elements is used since these connections need to be damaged and removed, producing significant demolition waste [3]. On the other hand, assembled structures can be successfully demounted and reconstructed if the connection is designed to be a dry connection, created by using plates, steel threaded bolts, hinges, dowels, and anchorage rods [4].

Few recent investigations have focused on demountable RC structural elements, aiming to simplify the applications of this new system. However, limited experimental research has been conducted using the dry connection system [5-8]. Different configurations were proposed for dry connections, such as using a horizontal steel connecter and high strength bolts for shear wall connection [5], where the load effectively transferred through the connection and the failure administrated by the resistance of the main walls while the connecter remains undamaged. Furthermore, other demountable connections between beam and column were introduced using steel endplate, steel angle, and steel tube connections [6], concluding that the steel end plate connection was the most effective assembly technique in terms of structural behaviour as the force directly transferred from the beam to the connection. Additional configuration of using an embedded rod and pretension bolts to connect beam and column was also proposed [7]. The test results showed that the connection exhibited an acceptable seismic performance compared to the cast-in-situ reinforced concrete beam-column joints. Furthermore, a dry joint connection between assembled slabs filled with aluminium foam was suggested, which is stiff enough to provide the shear transfer between the connected slabs [8].

Some other dry connection configuration was only proposed in the literature without physical proof of concept testing to assess the structural behaviour of the dry connection [9, 10]. For example, separate concrete blocks of prism shape mounted on the surface of the base and pulled together by horizontal strands, and anchor devices for fixing the support were proposed and tested by finite element model for demountable foundation [9]. In addition, a new configuration of demountable precast reinforced frame system consisting of steel plates/angles, steel plates/tubes, and high strength bolts were also suggested [10]. The proposed scheme included a solution for slab-to-slab, slab to beam, beam to column, column to column, and column foundation connections. However, the proposed demountable connections were not tested analytically nor experimentally to evaluate the structural behaviour of the connection.

The main aim of the paper is to present a proof of concept of an innovative, sustainable, demountable connections of structures, that would be adopted in industry and covered by codes of practice. Therefore, a new demountable, sustainable system for RC slabs is proposed, allowing easy assembly and disassembly for slab segments. The proposed demountable system for the reinforced concrete slabs was experimentally investigated to assess the structural behaviour of the connection. Two approaches were proposed and studied; the first connection system included edge-to-edge slab ends, while the other included a shear key at the connection section. The experimental tests included seven specimens; one slab was monolithic to serve as a control specimen, while the other six were cast separately. The slab segments were connected using top and bottom steel plates combined with high tensile threaded steel bolts. The effect of using stirrups at the connection section, using a shear key at the connection, bolt diameter, and number on the performance of the dry connection between slab elements is investigated.

2. Experimental programme

2.1 Test specimens

Seven simply reinforced concrete slabs were prepared and tested. The details of the reinforcement for the slabs tested are shown in Figs. 1 to 8. The slabs had a rectangular cross-section of 500×160 mm, while the total span length was 5200mm; 5000 mm for slab span and 100 as overhangs on each end. The slab reinforcement was chosen to typically represent the main and lateral slab reinforcement in a real slab floor, which was kept the same for all slabs. As the main objective of DfD system is to allow the reuse of structural elements at the end of the structure life, the corrosion resistance stainless-steel bars were used as internal reinforcement, instead of conventional less-corrosive resistance steel reinforcement, enhancing the life span of the structural elements. Five bars of Ø12 mm were used for the main longitudinal reinforcement, as illustrated in Fig. 1-b. In addition, Ø8 mm bars spaced at 150 mm at the bottom were chosen for the distribution reinforcement.

Table 1 presents the details of the specimens tested. For comparative purposes, one slab was designed as a monolithic RC control slab. At the same time, six specimens were demountable slabs, assembled by using top and bottom steel plates at the surfaces of the slab, which were then joined by using high tensile threaded steel bolts. Besides, steel ducts were installed inside the slabs before casting to hold the threaded bolts at the exact connection position.

Two different techniques with different parameters were employed to connect the two segments of each slab: a simple bolted connection and a shear key at the connection section. The examined parameters in this experimental investigation were the use of stirrups at the connection section, the availability and step size of a shear key at the connection, bolt diameter and number. Therefore, four specimens were designed with a shear key at the connection section, while two were designed without a shear key. The slab notations were identified according to the connection details, as listed in Table 1. The first two numbers identify the number (3 or 4) and diameter of the bolts (Ø8 or Ø12) while the third letter indicates the existence of the shear key, ‘K’ for using a shear key, and ‘NK’ for no shear key. Likewise, for specimens without a shear key, the fourth letter, ‘S’ or ‘NS’, shows the use or of stirrups and no steel stirrup, respectively. However, for specimens with a shear key, the fourth number indicates the step size of the key, ‘10’ for a shear key of 100mm step width, whereas ‘20’ for a shear key of 200mm step width.

Two specimens were designed to examine the effect of the stirrups at the connection section. The demountable slabs C-3-12-NK-S and C-3-12-NK-NS are shown in Figs. 2 and 3, respectively. Each specimen included two identical segments; the length of each part was 2600 mm, as shown in Figs. 2 (a) and 3 (a). The front view of the two slabs before and after assembly is shown in Fig. 4.

Furthermore, three specimens were designed using the same shear key step size of 100mm, with varying diameters and number of bolts. The details of C-3-12-K10, C-3-8-K10 and C-4-12-K10 are shown in Figs. 5 and 6. The slabs included two segments, one segment with a top concrete step and one with a bottom step, each 100 mm in width by 80 mm in depth. The total length of each element, including the step, was 2650 mm, as shown in Figs. 5(a), 5(b), 6(a) and 6(b). In addition, stirrups were used around the ducts at each slab segment to strengthen the connection section, as shown in Figs. 5(c) and 6(c). Finally, one specimen was designed with a wider shear step of 200mm to study the effect of shear step size on the connection performance. The total length of each slab segment with either bottom or top concrete step is 2700 mm, as shown in Fig. 7(a). Stirrups were used around the ducts at each slab segment, as shown in Fig. 7(c). Fig. 8 shows the slabs with a shear key before and after assembly.

2.2 Materials

Stainless steel bars were used for the reinforcement, mainly because of their corrosion resistance. The tensile strength of the reinforcement was found by testing three specimens, as summarized in Table 2.

The specimens were cast using ready-mix conventional concrete. The mix was designed with a target compressive strength of 35 MPa and maximum aggregate size of 20 mm. Three cubes were tested on each test day to find the average compressive strength for each slab specimen tested. In addition, two cylinders were tested to find the splitting tensile strength of each slab specimen at the test day.

The details of the connections included stainless steel plates of 8 mm thickness, steel bolts of high tensile strength grade 10.9 (tensile strength of minimum 1000MPa and yield strength up to 900MPa), mild-steel ducts, washers, and high tensile nuts of grade 10 (tensile strength of minimum 1000 MPa).

2.3 Test setup

The demountable slabs were connected by using top and bottom stainless-steel plates of 500 widths and 8 mm thickness that were pre-drilled at bolts locations before being placed on the top and bottom of the slab surfaces. Then, the slabs were assembled using fully threaded bolts of a total length of 250 mm, and a washer and nuts were attached to each bolt end. For consistency, a torque wrench was used to tighten the bolt by applying 120 Nm torque on bolts with 12 mm diameter and 40 Nm torque on 8 mm diameter bolts.

Fig. 9 shows the test setup of slabs. A steel spreader beam was employed under the 1000 kN hydraulic jack to transfer the main jack load to the two loading plates of 500 mm length, 150 mm width, and 40 mm thickness that were located on the surfaces of the slab at the load location using special grout material. The slabs were supported using end roller and hinge supports. In addition, three digital cameras were used to measure the crack width. One camera was positioned at the mid-span section of the slab, and the remaining two cameras were located at the loading location. Furthermore, seven linear variable differential transducers (LVDTs) were installed to record the deflection of the slabs throughout the tests. Top LVDTs were mounted at the end supports to detect possible loss of stability or deformation, whereas the remaining five LVDTs were installed underneath the slab to record vertical deflections at different locations as shown in Fig. 9. Two strain gauges were attached to the reinforcement surface at positions of the load application points. In addition, two more strain gauges were externally attached to both the top and bottom connection steel plates at the midspan. Special strain gauges were also used at the top of concrete surface (compression side) to measure the concrete strain during the test The displacement-controlled loading protocol was utilized in each test, with a constant loading rate of 0.09mm/sec throughout the testing. Continuous data logging was performed with the help of an electronic data logger.

3. Test results

3.1 Failure Modes

Fig. 10 shows the manually detected cracks for all slab specimens. All specimens exhibited the first cracking at the mid-span section between the two applied load regions under the effect of total applied load of 3 kN as the same batch of concrete were used in each test specimens, leading to a similar cracking moment capacity. Considering elastic theory, the total cracking load P_{cr} for each slab may be calculated from:

$$2P_{cr} = \frac{f_{ts}bh^2}{6a} \tag{1}$$

where f_{ts} is the flexural tensile strength of concrete $f_{ts} = 0.31\sqrt{f_c^{'}}$ [11], a is the shear span, b and h are the slab width and depth, respectively. The theoretical cracking loads obtained from the above formula are presented in Table 4, comparatively in agreement with the experimental cracking load of 3.0 kN.

As the applied load was increased further than 3 kN, flexural cracks were recorded along the slab span. The vertical flexural cracks slightly extended to the compression zone in all slabs tested, and the width of the existing cracks developed wider. However, there was no sign of any concrete crushing due to the actuator's deflection capacity limitation, which is around 200mm (Span/25). The additional reason for cracks not extending to the compression zone was the sudden failure documented in slabs C-3-12-NK-NS, C-3-12-NK-S, C-3-12-K10, and C-3-8-K10.

The mode of failure and the deformation shape of the slabs tested are shown in Figs. 11-1, 11-2 and 12, respectively. The failure mode initiated with vertical flexural cracks developed at the mid-span region between the two applied loads for all slabs tested, yet; those cracks were not fully extended to the compression zone because of the actuator deflection capacity for some specimens; control slab, C-3-12-K20, and C-4-12-K10. Therefore, those slabs were tested to the maximum actuator's deflection capacity regardless of achieving a failure point.

On the other hand, C-3-NK-NS, C-3-NK-S, C-3-12-K10, and C-3-8-K10 exhibited a sudden failure, where the main crack, detailed at the bolt line extended wider until unexpected failure was documented in these slabs. C-3-12-NK-S and C-3-12-K10 demonstrated one bolt tearing at the tension side of the slabs, as seen in Figs. 11-1(c) and 11-1(d), respectively. However, in slab C-3-8-K10, three bolts were torn at the tension and compression side along the main crack line because of the reduction in the bolt diameter from Ø12 to Ø8, as observed in Fig. 11-2(e).

The effect of step size on failure mode can be seen in slabs C-3-12-K10 and C-3-12-K20. Although both slabs were assembled using the same number/size of bolts, a different mode of failure was observed in each slab. Slab C-3-12-K10 recorded a sudden failure identified by one bolt tearing, while C-3-12-K20 continued to carry the load until the maximum actuator deflection capacity because of the stiffness improvement of the connected section caused by a wider step size. Furthermore, increasing the number of bolts showed similar behaviour to raising the shear key step size. Slab C-4-12-K10 with one more bolt than C-3-12-K10 at each bolt line shifted the failure mode from sudden failure to no failure point, owing to the tensile stress reduction of the four-bolt connection.

Alternatively, there was no significant difference in the failure mode using either stirrup or shear key at the connection section. Slabs with either stirrup or no stirrup at the connection section, C-3-12-NK-NS, and C-3-12-NK-S, showed a sudden failure due to the wide crack at the bolt line; however, one bolt tearing was recorded in slab specimen C-3-12-NK-S. This could be due to the additional stress concentration on each bolt caused by the enhancement of the total load capacity of the slab. In addition, C-3-12-K10 with a shear key, and C-3-12-NK-NS without a shear key, exhibited the same sudden mode of failure recognized by bolt tearing at maximum load capacity. Additionally, increasing the bolt diameter enhanced the mode of failure of the connected slabs. Using Ø12 in slab C-3-12-K10 rather than Ø8 in C-3-8-K20 moved the failure mode from three-bolt tearing to one bolt tearing due to the enhancement of the bolt resistance as the bolt diameter was increased.

3.2 Crack widths

Fig. 13 shows the average crack width against the total load of the slabs tested. The values of crack width were measured at the significant crack between the two applied load regions. The width of the main crack of the Control slab was generally lower than the demountable slabs at higher load values.

For simple bolted connections, the width of cracks for C-3-12-NK-NS and C-3-12-NK-S were higher than demountable slabs with a shear key at a higher load value, owing to the improvement of the shear resistance at the assembled section for slabs with a shear key. Moreover, adding stirrup to the assembled section did not improve the crack width in slab C-3-12-NK-S compared to C-3-12-NK-NS.

For slabs with a shear key, increasing either the number of bolts or the shear key step size has minimal effect on crack width. The crack width for C-4-12-K10 was almost the same as C-3-12-K10 until 86% of its maximum total load capacity. Also, the crack width for C-3-12-K20 was similar to C-3-12-K10 until 63% of its total load capacity; after that, the crack width of C-3-12-K10 developed wider. On the other hand, decreasing the number of bolts in C-3-8-K10 increased the crack width at failure because of the sudden failure recoded in this slab.

3.3 Strains in stainless steel reinforcement, concrete, and steel-plates

Fig.14 shows the stainless-steel tensile strain variation against the total applied load of the specimens tested. Adding stirrup, changing the shear-step size, and changing the number or diameter of bolts have no significant effect on the strain values of the stainless-steel reinforcement until the failure of each specimen, as the same amount of steel reinforcement for all slabs tested was used, resulting in similar behaviour.

Furthermore, steel yielding was only recorded in the Control slab at 90% of the total applied load, while no steel yielding was recorded for all demountable slabs. This is mainly attributed to the fact that all demountable slabs exhibited stiffness reduction, consequently, carried less load compared to the Control slab by at least 25.9%, implicating a reduced level of tensile stresses in the stainless-steel bars. Therefore, the yielding point could not be reached before failure.

Fig.15 illustrates the recorded strain values in concrete at the compression side. No concrete crushing was documented in all slabs tested, owing to the actuator deflection limit for not achieving failure point at some specimens; Control, C-3-12-K20, and C-4-12-K10. In addition to the sudden failure recorded in other slabs tested, C-3-NK-NS, C-3-NK-S, C-3-12-K10, and C-3-8-K10. Furthermore, changing the connection details has no significant effect on the measured strain values in concrete. All demountable slabs exhibited almost similar concrete strain values until reaching the maximum load as concrete properties of the slabs tested were almost similar.

The strain values of top and bottom steel plates of demountable slabs are presented in Fig.16. The recoded values were negative for top plates under compression and positive for bottom plates under tension. Adding stirrups to the assembled section has no effect on the strain values in either bottom or top steel plates. In addition, adding a shear key to the connected section, providing the right number of bolts and shear key step size, decreased the total recorded strain at the bottom and top steel plates. C-3-12-K10 with a shear key reduced the recoded strain compared to C-3-12-NK-NS with no shear key due to the enhanced stiffness of the connected section provided by the shear key. In addition, increasing the width of the shear key at the assembled section has a significant effect on reducing the total strain of the top and bottom connection plates; C-3-12-K20 recorded the lowest strain values among the slabs tested due to the use of a wider shear key step at the slab connection. Furthermore, increasing the number of bolts has a similar effect of increasing the shear key step size; C-4-12-K10 showed a lower strain value of the top and bottom steel plates at the same load than slab C-3-12-K10. On the other hand, slab C-3-8-K10 recorded the highest strain value at the top and bottom steel plates compared to other slabs with shear key because of reducing the bolt size from Ø12 mm to Ø8mm.

3.4 Total load capacity

The total load capacities for the slabs tested are listed in Table 4, indicating that the total load capacities for all connected slabs were lower than the monolithic slab because of stiffness reduction caused by discontinuity of the rotation at the connected section. For slabs with simple bolted connection, C-3-12-NK-NS and C-3-12-NK-S, the load capacities were 65% and 58% less than the Control slab, respectively. However, adding a stirrup to the connected section enhanced the total load capacity of C-3-12-NK-S by 42% compared to C-3-12-NK-NS due to the improvement in concrete confinement provided by the stirrup, consequently, improving the concrete compressive strength of the assembled section. In addition, adding a shear key to the demountable section, providing the correct number of bolts and shear key step size, improved the total load capacities of the demountable slabs due to the stiffness enhancement in the connected section. The improvement in the full load capacity after adding the shear key to C-3-12-K10 was 22% higher than C-3-12-NK-S with a simple bolted connection. However, increasing the shear key step of C-3-12-K20 reduced the total load capacity by 6% compared to C-3-12-K10 due to the critical wide crack developed in C-3-12-K20 at failure.

Moreover, increasing the number of bolts seemed to improve the total load capacity of slabs tested while decreasing the bolt diameter recorded a reverse effect. C-4-12-K10, with a shear key and one more bolt per bolt line than C-3-12-K10, improved the load capacity by 24%. Conversely, using a smaller bolt diameter, Ø8 instead of Ø12, in slab C-3-8-K10 reduced the load capacity by 59% compared to C-3-12-K10.

3.4.1 Theoretical prediction of load capacity

The simplified rectangular stress distribution proposed by the Structural Eurocodes [12] can be used to predict the flexural moment capacity of the monolithically casted slab. Considering the strain compatibility and force equilibrium, the neutral axis depth can be obtained from:

$$x = \frac{A_s f_y}{\lambda \eta f_{ck} b} \quad (2)$$

where A_s and f_y are the area and yield strength of the main longitudinal bottom steel, λ (=0.8 for $f_{ck} \leq 50MPa$) and η (=1.0 for $f_{ck} \leq 50MPa$) are two coefficients defining the effective height and effective strength of the simplified, equivalent rectangular stress distribution, respectively. The moment capacity of the slab M_m can be found by the steel reinforcement tensile force as below:

$$M_m = A_s f_y (d - \frac{\lambda x}{2}) \quad (3)$$

where d is the slab effective depth. Eqs. (2) and (3) were based on yielding of main longitudinal bottom steel reinforcement, that was clearly satisfied at failure as depicted in Fig. 13. Therefore, the moment capacity of the control slab, obtained from Eqs. (2) and (3), is 40.44 kNm, agreeing well with the experimental moment capacity of 42.8 kNm.

The fact that there is a duct to hold the bolts at their locations creates high-stress concentration accompanied by a reduction of the concrete slab section. Therefore, the method mentioned above to find the flexural moment capacity for the demountable slabs seems inaccurate. The slab section along the bolts is clearly controlling the moment capacity of demountable slabs as it appeared to be the weakest section. Fig. 17(a) shows the compression and tension forces transferred through the top and bottom steel plates. These forces are in equilibrium and, consequently, equal and could be found by:

$$F_c = F_t = \frac{M_m}{z} \tag{4}$$

where F_c and F_t are the top and bottom forces in the steel plates, respectively, M_m is the moment at the mid-span section and z is the distance between the top and bottom steel plates. Note that depending on the gap between the two slab segments, part of the top compression force would be resisted by concrete. However, this concrete compression contribution is ignored, providing more critical design for the slab flexural capacity.

The bolts are responsible for transferring these forces to the demountable slab, producing compression force on one side of the slab and tensile force on the other side as shown in Fig. 17(b). Consequently, the tensile stresses f_t in concrete caused by the bolts could be estimated from:

$$f_t = \frac{F_t}{A_{net}} \tag{5}$$

where ($A_{net} = (b - n\phi)h$) is the net section area of concrete (see Fig.17 (c)), b and h are the width and depth of the slab, and, n and ϕ is the number and diameter of ducts, respectively. When the tensile stresses f_t reach the concrete tensile strength, the moment capacity M_m of the slab section may be calculated using Eq. 6:

$$M_m = F_t z = f_{ts} A_{net} z \tag{6}$$

Table 4 shows the ratio of the experimental to predicted moment capacities as found from Eq. (6). Generally, the predicted results using Eq. (6) demonstrate a sufficient agreement with the experimental results, implying the applicability of Eqs. (4) to (6) for predicting the moment capacity of demountable slabs. However, more advanced techniques considering full modelling and simulation of various elements at the demountable joint, for example nonlinear finite element analysis, may be considered to overcome some of the simplification and assumptions of Eqs. (4) to (6), above.

3.5 Load-displacement curves

Five linear variable differential transducers (LVDTs) were used under the slabs at different locations to measure the deflection of the slabs throughout the tests. Since the lowest load value among the slabs tested was 10.3 kN, this value was chosen to create the deflection curve along each slab span to compare the deflection profile for all slabs tested, as shown in Fig. 18. The significant deflection value for all slabs tested was recorded in the mid-span section. Therefore, the relationship between the total applied load and the mid-span deflection is plotted in Fig.19. However, the two LVDTs at the support were not presented because no settlement was recorded.

The load-deflection curve started with a linear response until the first crack at 3 kN for all slabs tested. While after cracking, there was an apparent reduction in the flexural stiffness that was more dominant in the demountable slabs than in the Control slab. For slabs with simple bolted connection, C-3-12-NK-NS and C-3-12-NK-S, there was a significant drop in the flexural stiffness compared to the Control slab. Though, adding stirrups to the assembled section improved the flexural stiffness and the total load capacity of the slabs tested by 42% because of the improvement in the concrete compressive strength caused by concrete confinement provided by stirrups.

Demountable slabs connected by shear key showed more flexural stiffness than slabs with simple bolted connections, except for C-3-8-K10. Slab C-3-12-K10 with a shear key indicated a noticeable enhancement in the flexural stiffness compared to C-3-12-NK-S, because of the improvement in the shear resistance provided by the shear key. Furthermore, increasing the shear key step size improved the flexural stiffness of C-3-12-K20 over C-3-12-K10 for some limits. Both slabs have almost the same flexural stiffness until 23% of the maximum total load of slab C-3-12-K10. After that, there was a clear stiffness enhancement for slab C-3-12-K20 until 78% of the total load of slab C-3-12-K10 as the cracks were not dominant at low load values; therefore, there was no pronounced effect of the shear key step size. On the other hand, at higher load values and wider cracks, the flexural resistance improved due to the increase in the shear key step size at the assembled section. Afterwards, the flexural stiffness dropped in C-3-12-K20 owing to the larger crack width compared to C-3-12-K10.

Increasing the number of bolts decreased the flexural stiffness of the demountable slabs to some extent. Slab C-4-12-K10 showed slightly lower stiffness than C-3-12-K12 until 77% of the maximum total load of slab C-4-12-K10 due to the bolts' position being distributed evenly at the edge and center in C-3-12-K10. In contrast, for C-4-12-K10, the bolts were distrusted at the section edge with no middle bolt. Furthermore, reducing the bolt size from Ø12 mm to Ø8 mm in slab C-3-8-K10 considerably decreased the flexural stiffness of the slab due to the reduction in the bolt resistance as the bolt diameter was reduced.

3.5.1 Theoretical prediction of load-deflection

The deflection (Δ) at the mid-span location for continuous slab under two-points load is found by Eq. (7):

$$\Delta = \frac{Pa\,(3L^2 - 4a^2)}{24E_c I_e} \tag{7}$$

where P is the span load, a is the distance between the support and loading point, L is the span length, E_c is the modulus of elasticity of concrete ($\approx 4700\sqrt{f_c'}$; f_c' is the cylinder concrete compressive strength in MPa) and I_e is the effective moment of inertia of the concrete cross-section. The effective moment I_e of inertia is equal to the gross moment of inertia, I_g, before cracking (Eq. (8)), while it can be expressed by Eq. (9) after cracking [13].

$$I_e = I_g \qquad M_a \leq M_{cr} \tag{8}$$

$$I_e = \frac{I_{cr}}{1 - \left(1 - \frac{I_{cr}}{I_g}\right)\left(\frac{M_{cr}}{M_a}\right)^2} \leq I_g \qquad M_a > M_{cr} \tag{9}$$

where I_{cr} is the cracked moment of inertia, obtained from elastic analysis of the transformed cracked section, M_a is the applied moment and M_{cr} is the cracked moment of the section (= $f_{ts}I_g/y$, f_{ts} is the concrete tensile strength, y is the distance from the centroid of the gross section to tension face, neglecting reinforcement).

The mid-span deflection for the control specimen can be predicted by Eq. (7). However, the mid-span deflection of demountable slabs cannot be found using Eq. (7) because of the discontinuity of the slab slope at the mid-slab section because of the top and bottom connecting steel plates, which results of a partial rotation at the midspan section, as shown in Fig. 20. The detailing of the demountable slabs controls the degree of rotation, such as the steel plate rigidity, the fixing bolts, and cracks in the area of connection. Consequently, for slabs with demountable connection the mid-span deflection could be calculated using Eq. (10):

$$\Delta = \frac{Pa\,(3L^2 - 4a^2)}{24E_c I_e} + \theta_m \frac{L}{2} \tag{10}$$

where θ_m is the rotation at midspan to the left or right of the demountable connection, as shown in Fig. 20.

Since the rotation value controlled mainly by the connection details, θ_m varied depending on the connection details. Therefore, θ_m, was firstly found for each slab by using the value of the experimental deflection value Δ in Eq. (10). The value of θ_m was found for each load value up to 70% of the total load capacity (slab's serviceability limit state), then the obtained results was plotted against each load value to find the best linear regression, as shown in Fig. 21 and listed in Table 5. The validity of the linear regression was tested by conducting the Pearson correlation test to measure the linear correlation between the experimental load and the mid-span rotation using SPSS software, as listed in Table 6. Pearson correlation has a rate between (-1 to 1), where a value of (-1) means a negative linear correlation. While a value of (0) implies no correlation, and + 1 signifies a total positive correlation. As listed in Table 6, the range for Pearson correlation coefficients between the experimental load and rotation 0.861 to 0.99, which is significant, and the correlation coefficient is significantly much less than the 0.05 margin, meaning that the linear correlation between the two variables is statistically significant at a 95% confidence level. Consequently, the linear correlation between the experimental rotation and the load is statistically considerable. As a result, the linear regression model can be assumed to be a good model for all data.

Fig.21 shows that the rotation value for demountable slabs with key, C-3-12-K20 and C-3-12-k10, was the lowest among the specimens tested, respectively. These results confirm that adding a shear key to the demountable slabs section improved the flexural stiffness and diminished the rotation value of slabs segments, agreeing with the experimental results. However, a small variation can be noticed for all slabs connection, except for C-3-12-NK-NS and C-3-8-K10, which recorded a sudden failure. Therefore, the mid-span rotation was estimated to be the average value of the obtained estimates in Fig. 21 as computed by:

$$\theta_m = \frac{2P}{812.2} \tag{11}$$

Comparison between the predicted and the experimental load-deflection at the mid-span section by using Eqs. (7) and (11) is shown in Fig. 22. The experimental and predicted results were in good agreement for the continuous slab until almost 75% of the total maximum load. However, using the same equation significantly underestimated the predicted deflection at higher load values. On the other hand, for the demountable slabs, Eq. (7) significantly underestimated the predicted deflection because of the assumption of continuity of the slab slope at the mid-span section. Therefore, the prediction calculated by Eq. (10) was approximately fitted to the experimental deflection by using the adjusted mid-span rotation values determined by Eq. (11). As a result, there is an improved agreement between the experimental results and the deflection prediction using Eq. (10), as shown in Fig. 22, verifying the validity of the proposed Eqs. (10) and (11) to predict the deflections of demountable slabs.

4. Conclusions

Design for deconstruction (DfD) using dry connection approach has been investigated in this paper. Seven full-scale slabs were prepared and tested; one slab was monolithic, while the other six slabs were connected using a simple bolted connection and a shear key. Different parameters were investigated including the availability of stirrups at the connection section, a shear key at the connection and, diameter and number of bolts. The main aim is to present a proof of concept of an innovative, sustainable, demountable connections of reinforced concrete structures, that would be adopted in industry and covered by codes of practice. Overall, the stiffness and capacity of slabs with dry demountable connections were less than the control, monolithic specimen. However, it is expected that such dry connections would allow future reuse of slabs at the end of life of structures, achieving more efficient use of resources and a significant reduction in demolition waste and cost. The following conclusions can be drawn based on the performance of various dry connection layouts:

- Using a shear key at the assembled section in demountable slabs is more efficient than using the simple bolted connection in terms of flexural stiffness, load capacity, and deflection.
- Adding stirrups to the assembled section enhanced the flexural stiffness and the load capacity of demountable slabs. However, there was no effect on the mode of failure or recorded strains in reinforcement, concrete and steel plates.
- Increasing the shear key step size improved the flexural behavior of the demountable slabs by enhancing the flexural stiffness, shifting the mode of failure from sudden, brittle to more stable, ductile failure and reducing the strain values in the top and bottom steel plates.
- Increasing the number of bolts slightly decreased the flexural stiffness of demountable slabs; however, it increased the load capacity, reduced the strain value in the top and bottom steel plates, and shifted the mode of failure from sudden to more stable.
- The moment capacity prediction of demountable slabs has shown a good agreement with the experimental results, emphasizing the significance of various elements of demountable dry connections.
- The deflection prediction of demountable slabs using the proposed technique has also shown a good agreement with experimental results.

Data Availability

The raw/processed data required to reproduce these findings cannot be shared at this time as the data also forms part of an ongoing study.

Acknowledgement

This work was supported by an Institutional Links grant, ID 414633184, under the Newton-Kâtip Çelebi Fund partnership. The grant is funded by the UK Department for Business, Energy and Industrial Strategy and TÜBİTAK – Scientific and Technological Research Council of Turkey and delivered by the British Council. For further information, please visit www.newtonfund.ac.uk.

References

1. Guy, B., S. Shell, and H. Esherick, *Design for deconstruction and materials reuse.* Proceedings of the CIB Task Group, 2006. **39**(4): p. 189-209.
2. Huang, W., et al., *Seismic performance analysis of a novel demountable precast concrete beam-column connection with multi-slit devices.* Journal of Building Engineering, 2021. **44**: p. 102663.
3. Xiao, J., T. Ding, and Q. Zhang, *Structural behavior of a new moment-resisting DfD concrete connection.* Engineering Structures, 2017. **132**: p. 1-13.
4. Fayyad, T. and A. Abdalqader, *Demountable reinforced concrete structures: A review and future directions.* 2020.
5. Sun, J., H. Qiu, and Y. Lu, *Experimental study and associated numerical simulation of horizontally connected precast shear wall assembly.* The structural design of tall and special buildings, 2016. **25**(13): p. 659-678.
6. Aninthaneni, P., et al. *Experimental investigation of dry beam-column moment connections for demountable precast concrete frame buildings*. in *Proc., New Zealand Society for Earthquake Engineering Annual Conf.(NZSEE)*. 2016.
7. Thomas, H.-K.K. and D.J. Lee, *Special precast beam-column connection using pure dry cast method.*
8. Weiss, G.C., *Demountable concrete buildings, structural design of floor slabs with concrete elements and aluminium foam*, in *Advances in Construction Materials 2007*. 2007, Springer. p. 697-709.
9. Sabitov, L., et al. *Development and investigation of the stressed-deformed state of the demountable foundation for support*. in *IOP Conference Series: Materials Science and Engineering*. 2017. IOP Publishing.
10. Aninthaneni, P. and R. Dhakal. *Demountable Precast RC frame building system for seismic regions*. in *International conference on earthquake engineering and seismology (IZIIS-50). Kiel, Germany*. 2015.
11. Belarbi, A. and T.T. Hsu, *Constitutive laws of concrete in tension and reinforcing bars stiffened by concrete.* Structural Journal, 1994. **91**(4): p. 465-474.
12. EC, *1-2: 2004 Eurocode 2: Design of concrete structures-Part 1-2: General rules-Structural fire design.* European Standards, London, 2004.
13. Bischoff, P.H., *Deflection calculation of FRP reinforced concrete beams based on modifications to the existing Branson equation.* Journal of Composites for Construction, 2007. **11**(1): p. 4-14.

Tables

Table 1: Details of slabs tested.

Slab notation	Connection with key	Stirrup at the connection	Number of parts	İdentical parts	Number of bolts	Bolts diameter (mm)
Control	N.A	N.A	N.A	N.A	N.A	N.A
C-3-12-NK-NS	no	no	2	yes	3	12
C-3-12-NK-S	no	yes	2	yes	3	12
C-3-12-K10	yes	yes	2	no	3	12
C-3-8-K10	yes	yes	2	no	3	8
C-4-12-K10	yes	yes	2	no	4	12
C-3-12-K20	yes	yes	2	no	3	12

Table 2: Mechanical properties of the reinforcement bars.

Bar size	Area (mm2)	Yielding strength (MPa)	Ultimate strength (MPa)	Modulus of elasticity (GPa)	Ultimate strain %
12 mm	113.1	573	784	143	0.14
8 mm	50.3	700	851	139	0.14

Table 3: Concrete properties of the slabs tested at the day of each slab test

Slab notation	f_{cu} (MPa)	f_c' (MPa)	f_{ct} (MPa)
Control	40.6	34.5	2.4
C-3-12-NK-NS	44.9	38.2	2.9
C-3-12-NK-S	44.7	38.0	2.7
C-3-12-k10	43.6	37.1	2.8
C-3-8-k10	47.4	40.3	3.0
C-4-12-k10	51.3	43.6	3.3
C-3-12-k20	49.3	41.9	2.8

f_{cu}*: is the cube compressive strength,* f_c' *: is the equivalent cylinder compressive strength assumed equal to* $0.85f_{cu}$*: ,* f_{ct} *is the concrete tensile strength by cylinder splitting test.*

Table 4: Crack width, total failure load, theoretical capacity predictions and mode of failure of the slabs tested.

Slab notation	The cracking load (kN)	Crack width (mm)		Total load (kN)	Shear load of bolts at failure	Experimental Moment capacity (kN.m)	Predicted moment capacity (kN.m)	Ratio of experimental/ predicted moment capacities	Mode of failure
		At max load	At max actuator deflection						
Control	3.76	1.4	1.4	42.8	-	42.8	41.2	1.04	Loaded until the maximum actuator deflection
C-3-12-NK-NS	3.96	6.92	6.92	14.6	47.4	14.6	22.6	0.65	Sudden flexural failure
C-3-12-NK-S	3.95	8.05	8.05	20.9	47.3	20.9	22.6	0.93	One bolt tearing
C-3-12-K10	3.90	2.36	6.01	25.5	46.7	25.5	22.3	1.14	One bolt tearing
C-3-8-K10	4.06	22.45	22.45	10.3	50.0	10.3	23.8	0.43	Three bolt tearing
C-4-12-K10	4.23	2.94	3.82	31.7	37.0	31.7	23.5	1.35	Loaded until the maximum actuator deflection
C-3-12-K20	4.14	5.74	15.6	23.9	49.7	23.9	23.7	1.01	Loaded until the maximum actuator deflection

Table 5: Predicted mid-span rotation with the total experimental load

Slab notation	mid-span rotation, θ_m
C-3-12-NK-NS	$\theta_m = (2/535)\mathrm{P}$
C-3-12-NK-S	$\theta_m = (2/705.11)\mathrm{P}$
C-3-12-K10	$\theta_m = (2/1139.3)\mathrm{P}$
C-3-8-K10	$\theta_m = (2/339)\mathrm{P}$
C-4-12-K10	$\theta_m = (2/877.87)\mathrm{P}$
C-3-12-K20	$\theta_m = (2/1277.1)\mathrm{P}$

Table 6: Pearson correlation coefficient computed using the experimental rotation and load

Slab notation			Rotation	Load
C-3-12-NK-NS (N=978)	Rotation	Pearson Correlation	1	0.972**
		Sig. (2-tailed)		0.000
	Load	Pearson Correlation	0.972**	1.00
		Sig. (2-tailed)		
C-3-12-NK-S (N=1121)	Rotation	Pearson Correlation	1	0.961**
		Sig. (2-tailed)		0.000
	Load	Pearson Correlation	0.961**	1.00
		Sig. (2-tailed)	0.000	
C-3-12-K10 (N=1194)	Rotation	Pearson Correlation	1	0.99**
		Sig. (2-tailed)		0.000
	Load	Pearson Correlation	0.99**	1.0
		Sig. (2-tailed)	0.000	
C-3-8-K10 (N=843)	Rotation	Pearson Correlation	1	0.95**
		Sig. (2-tailed)		0.000
	Load	Pearson Correlation	0.95**	1.00
		Sig. (2-tailed)	0.000	
C-4-12-K10 (N=1429)	Rotation	Pearson Correlation	1.00	0.984**
		Sig. (2-tailed)		0.000
	Load	Pearson Correlation	0.984**	1.00
		Sig. (2-tailed)	0.000	
C-3-12-K20 (N=1010)	Rotation	Pearson Correlation	1.00	0.864**
		Sig. (2-tailed)		0.000
	Load	Pearson Correlation	0.864**	1.0
		Sig. (2-tailed)	0.000	

**. Correlation is significant at the 0.01 level (2-tailed). N: is the sample size.

Figures

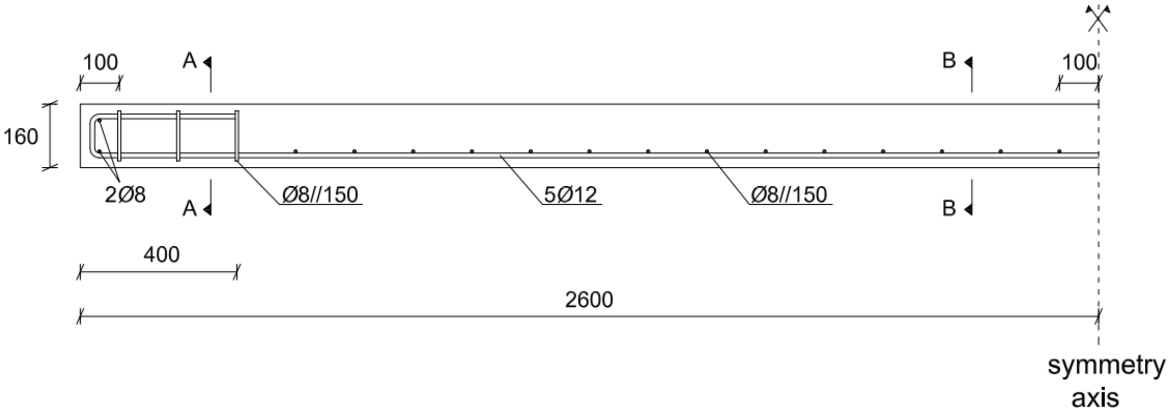

a. **Longitudinal reinforcement details section**.

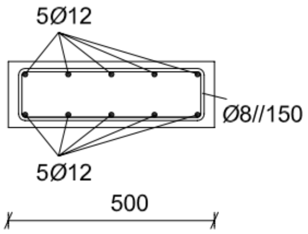

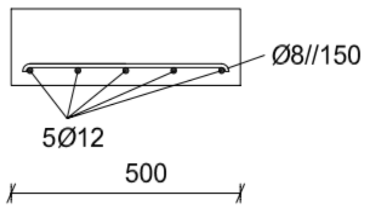

b. Side view A-A

c. Side view B-B

Figure 1: Reinforcement details of Control slab(dimentions in mm)..

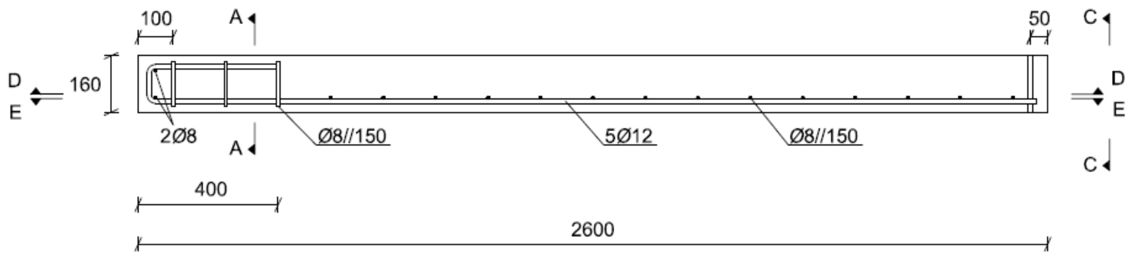

a. Front view.

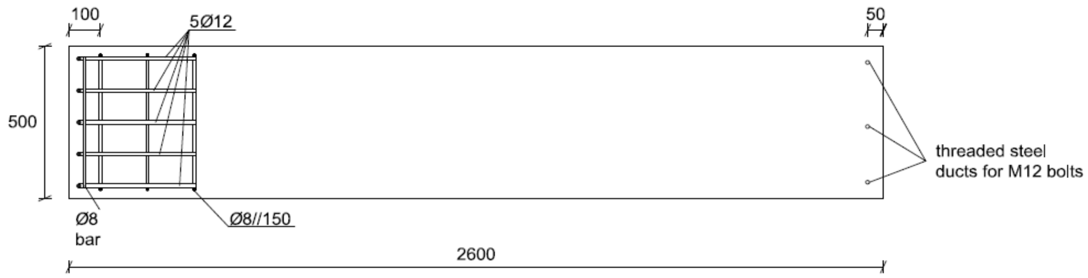

b. Top view D-D

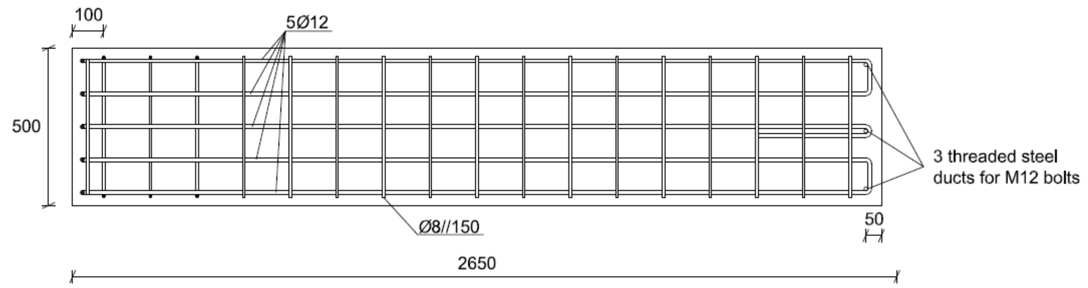

c. Top view E-E

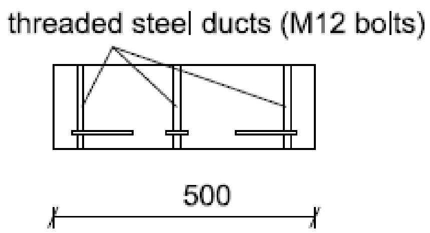

d. Side view C-C

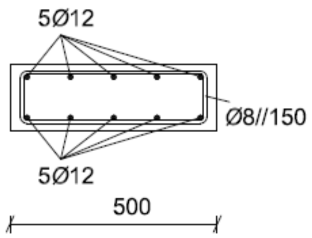

e. Side view A-A

Figure 2: Reinforcement details for slab C-3-NK-NS

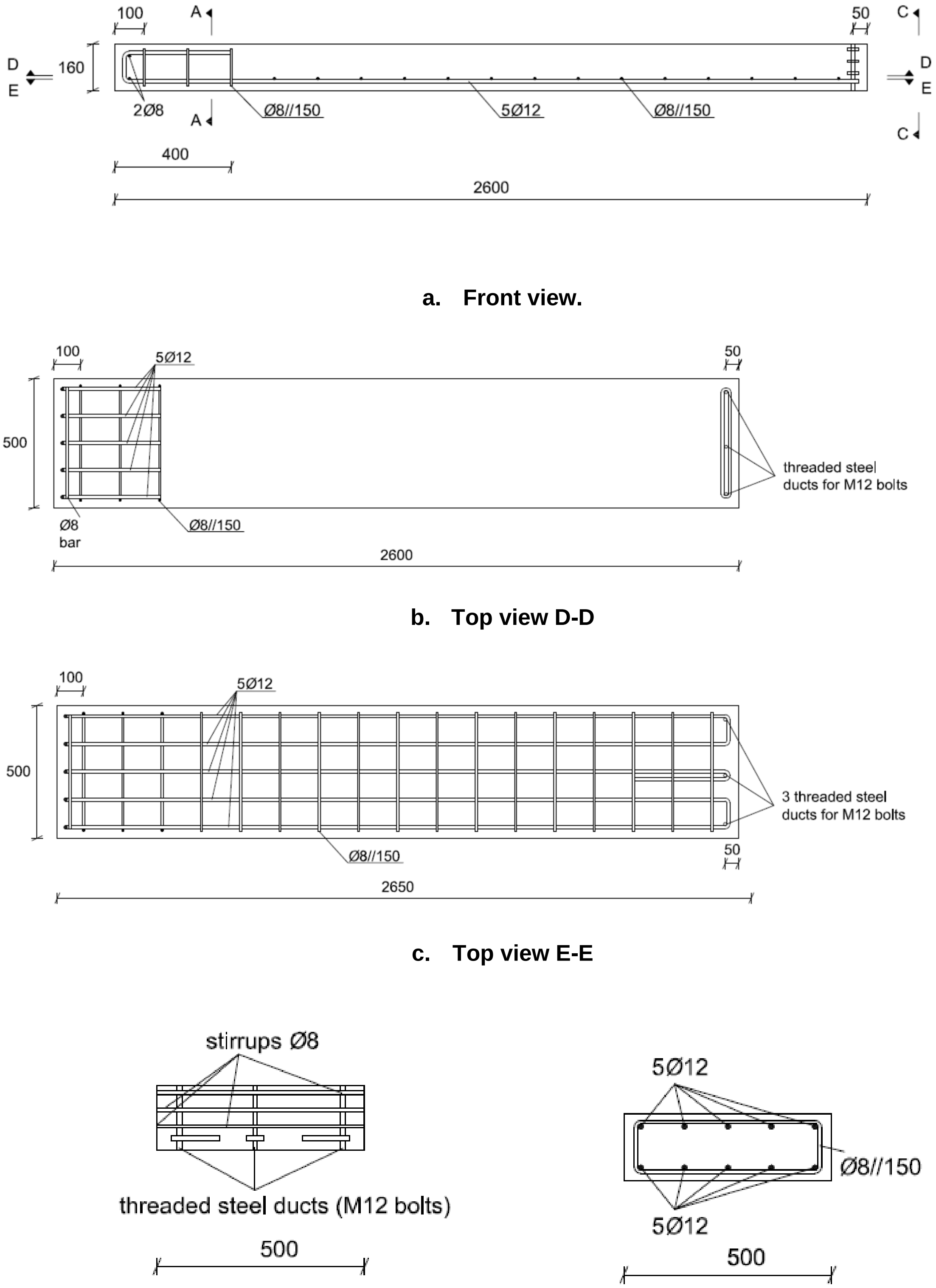

a. Front view.

b. Top view D-D

c. Top view E-E

d. Side view C-C

e. Side view A-A

Figure 3: Reinforcement details for slab C-3-NK-S.

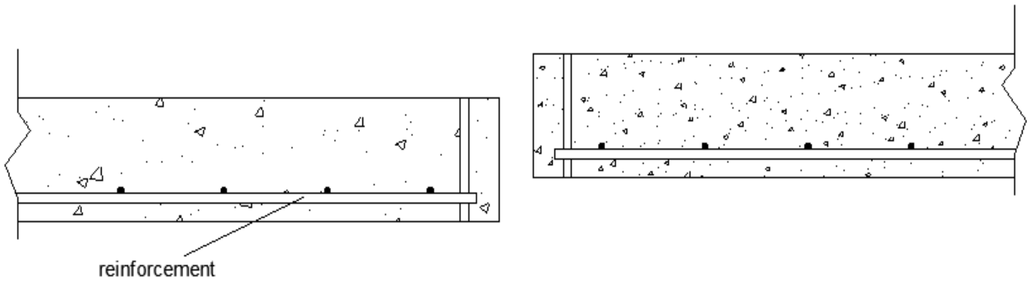

a. Before assembly

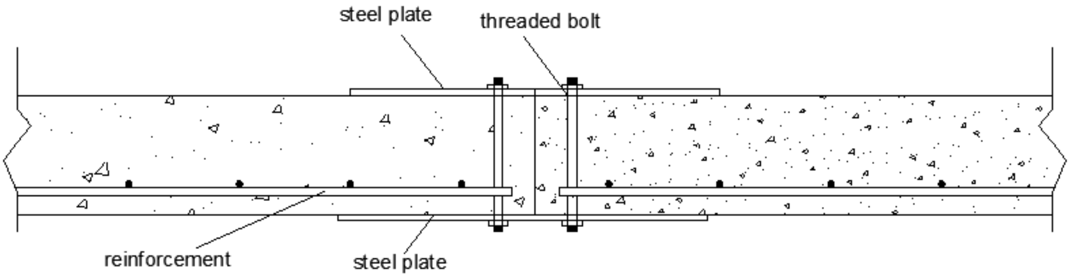

b. After assembly

Figure 4: Connection details for slabs with no key.

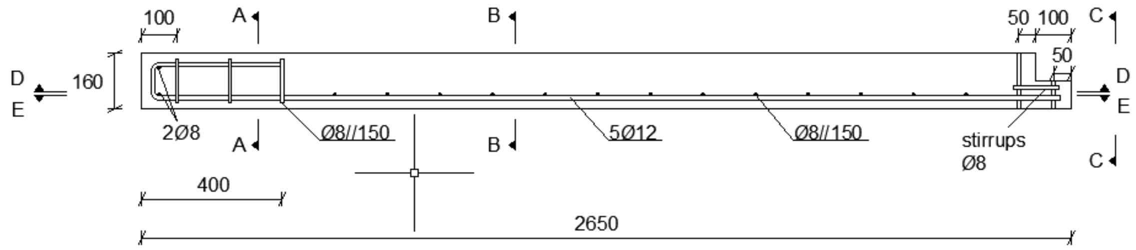

a(1). bottom step

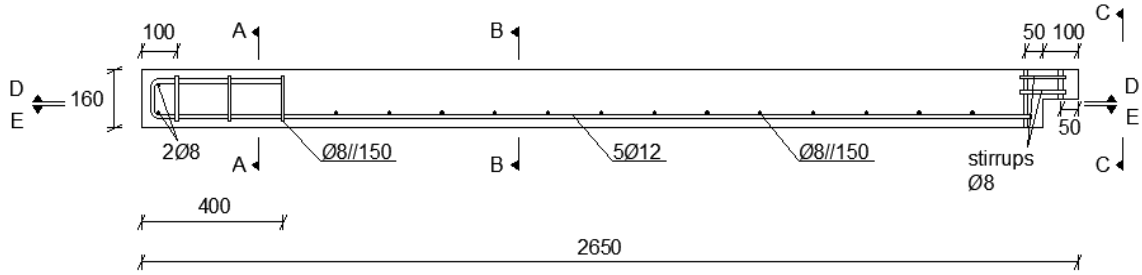

a(2). top step

a. Front view.

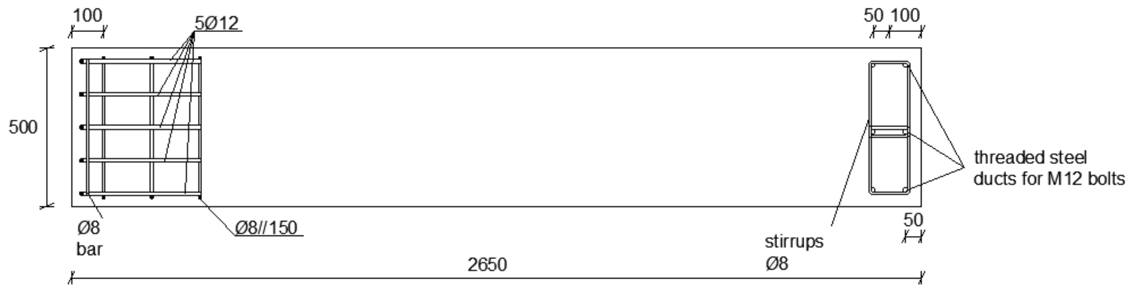

b (1).Top view D-D

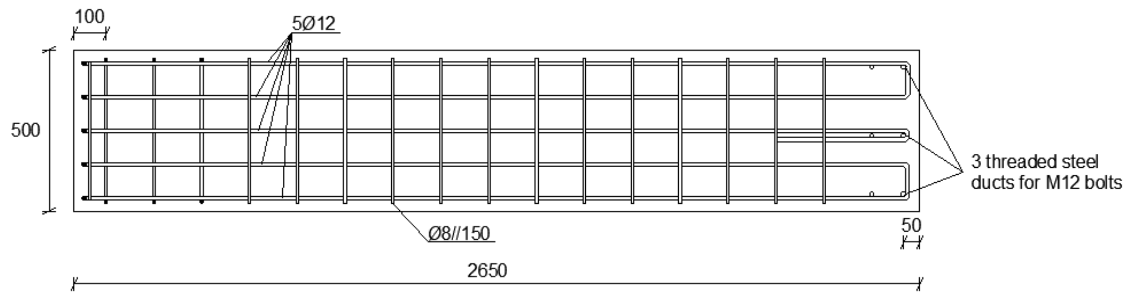

b (2). Top view E-E

b. Top view

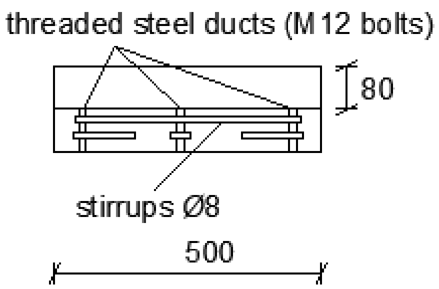

c (1). bottom step

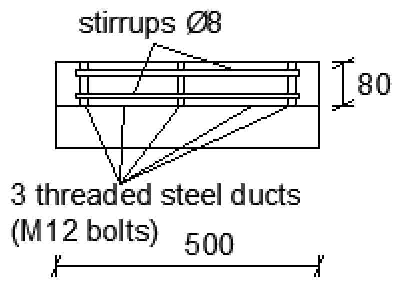

c (2). top step

c. Side view C-C

Figure 5: Reinforcement details of C-3-12-K10 and C-3-8-K10.

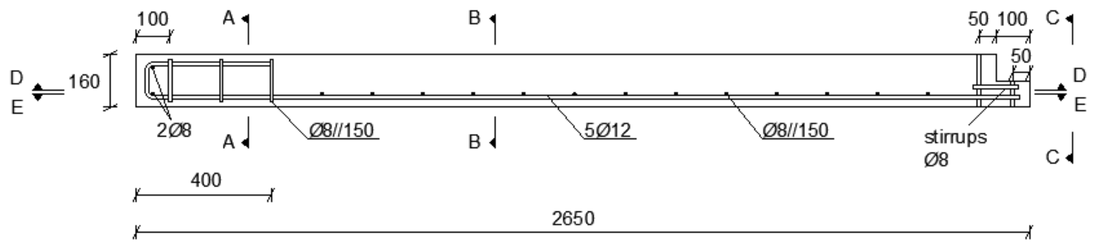

a(1). bottom step

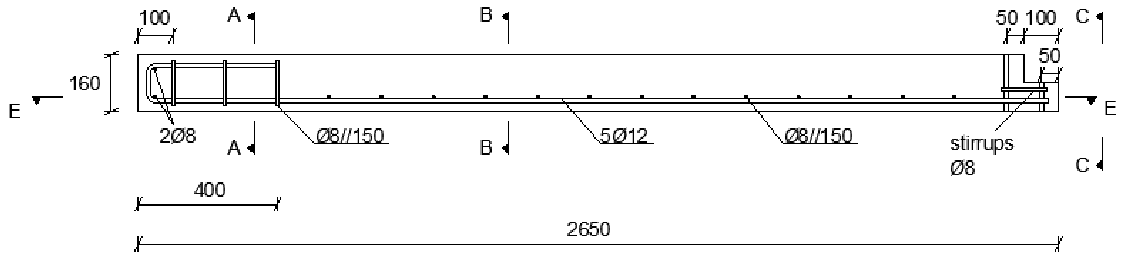

a(2). top step

b. Front view.

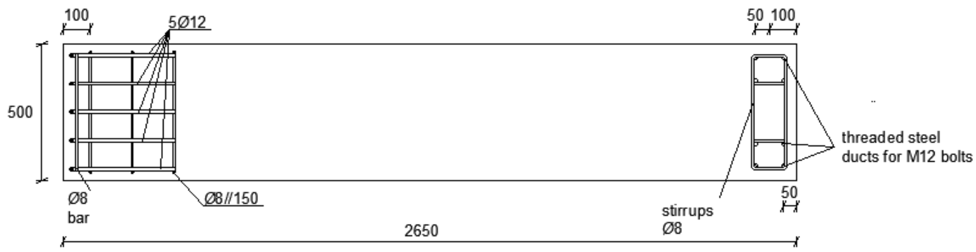

b (1).Top view D-D

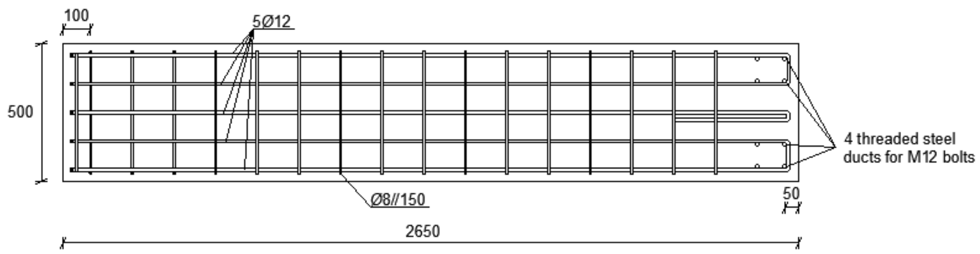

b (2). Top view E-E

b. Top view

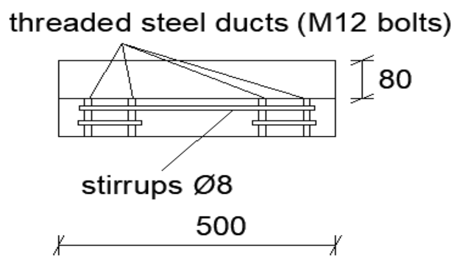

c (1). bottom step

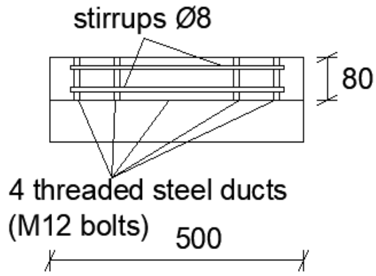

c (2). bottom step

c. Side view C-C

Figure 6: Reinforcemnt details of C-4-12-K10.

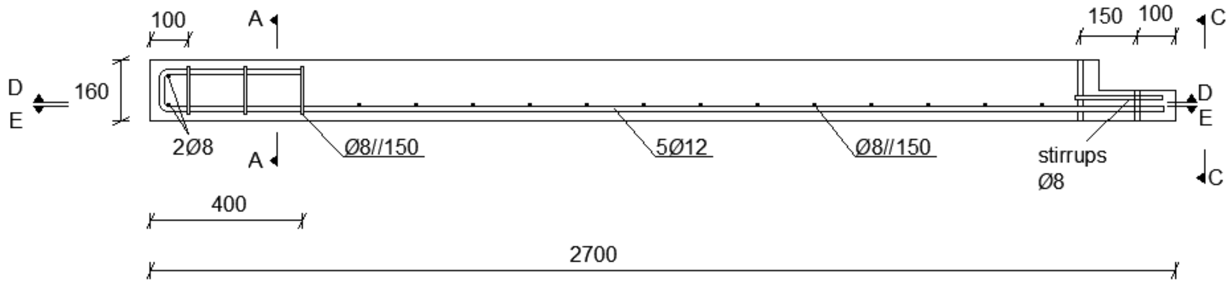

a(1). bottom step

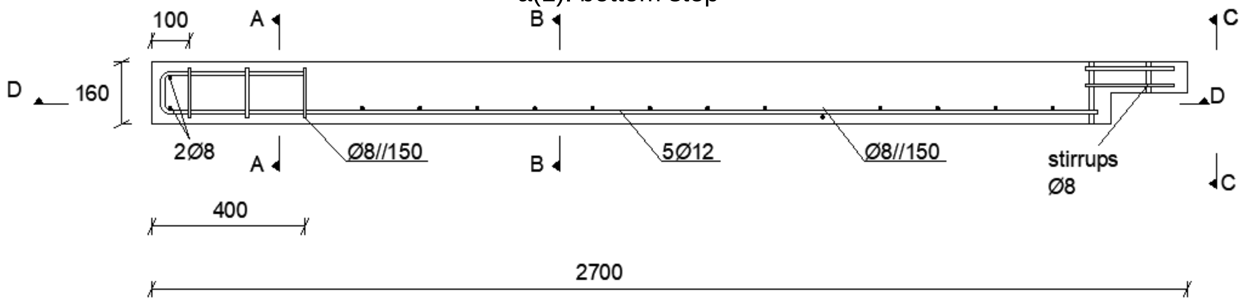

a(2). top step

a. Front view.

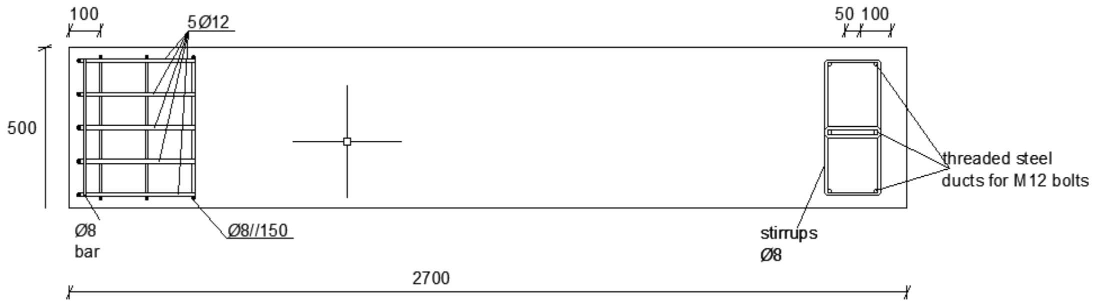

b (1).Top view D-D

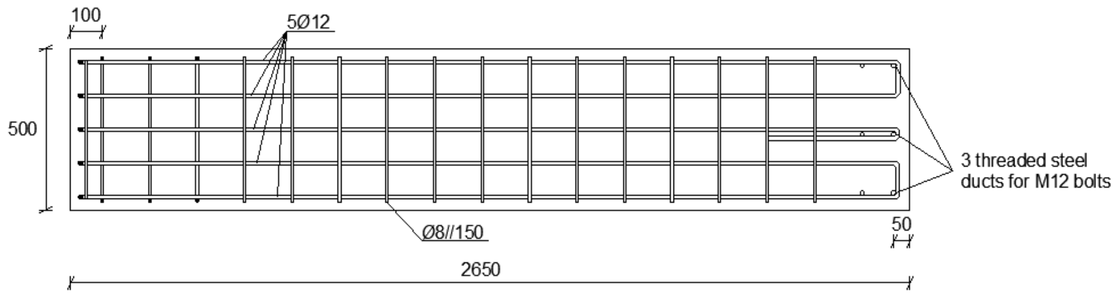

b (2). Top view E-E

b. Top view

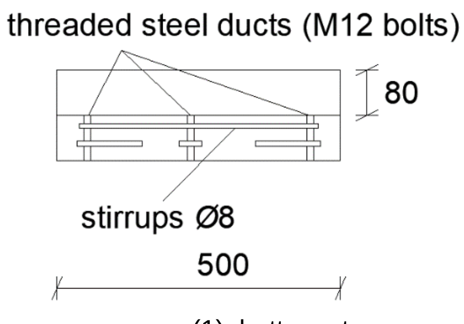

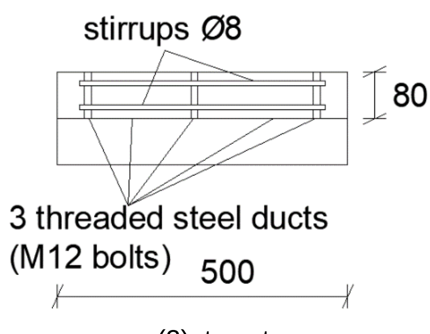

c (1). bottom step c (2). top step

d. Side view C-C

Figure 7: Reinforcement details of of C-3-12-K20.

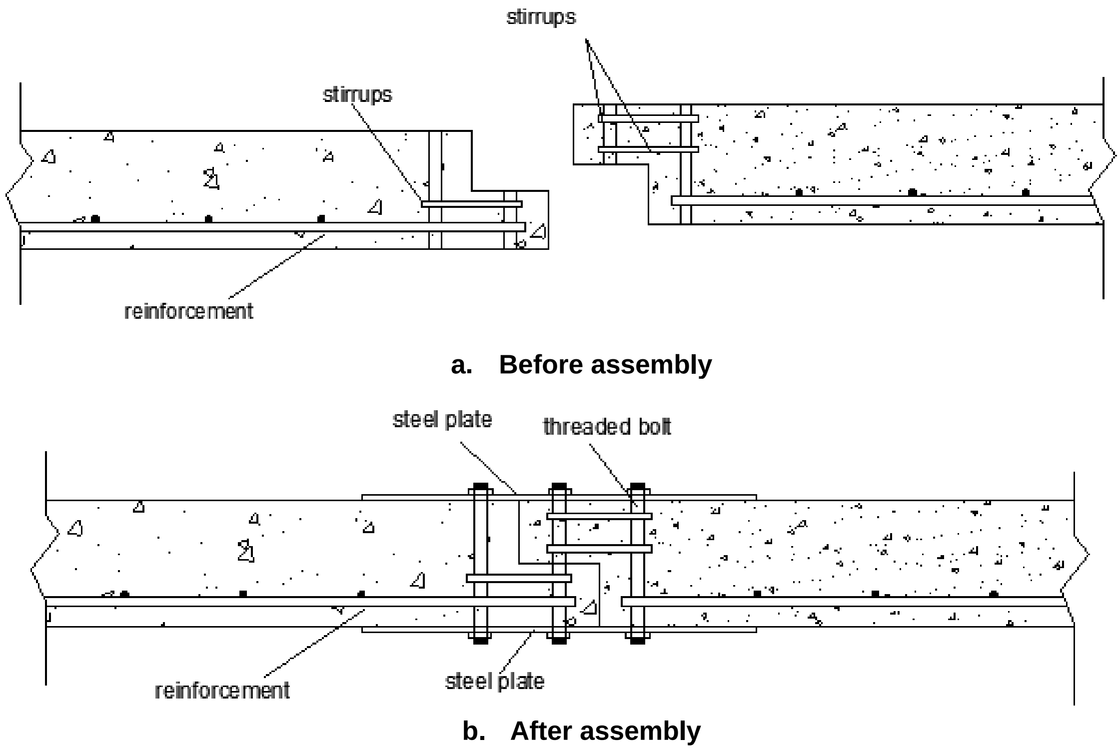

a. Before assembly

b. After assembly

Figure 8: Connection details of the slabs connected with a shear key.

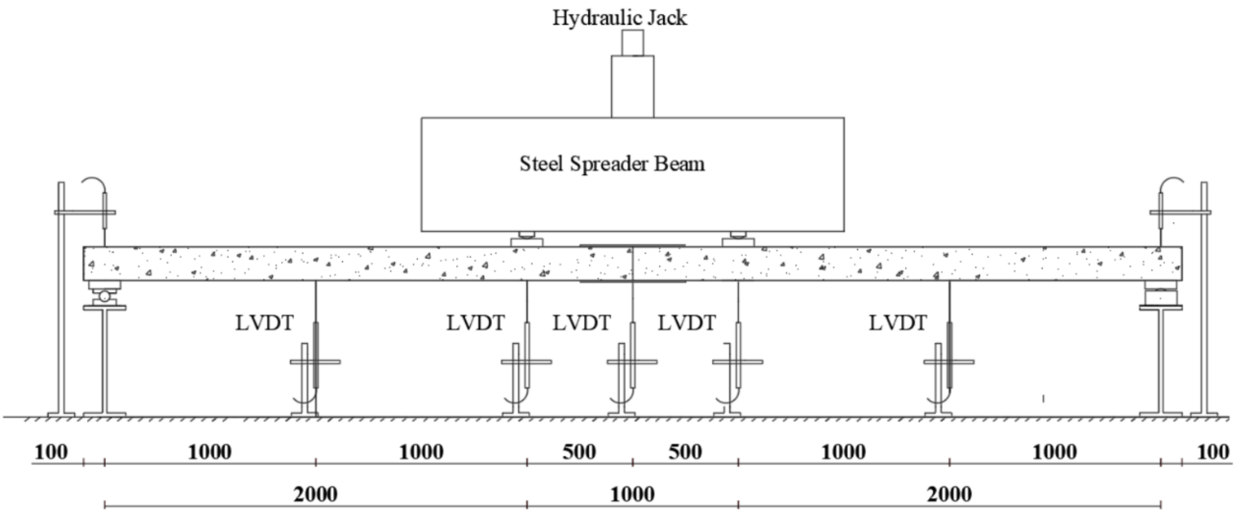

Figure 9: Experimental slab test setup (dimentions in mm).

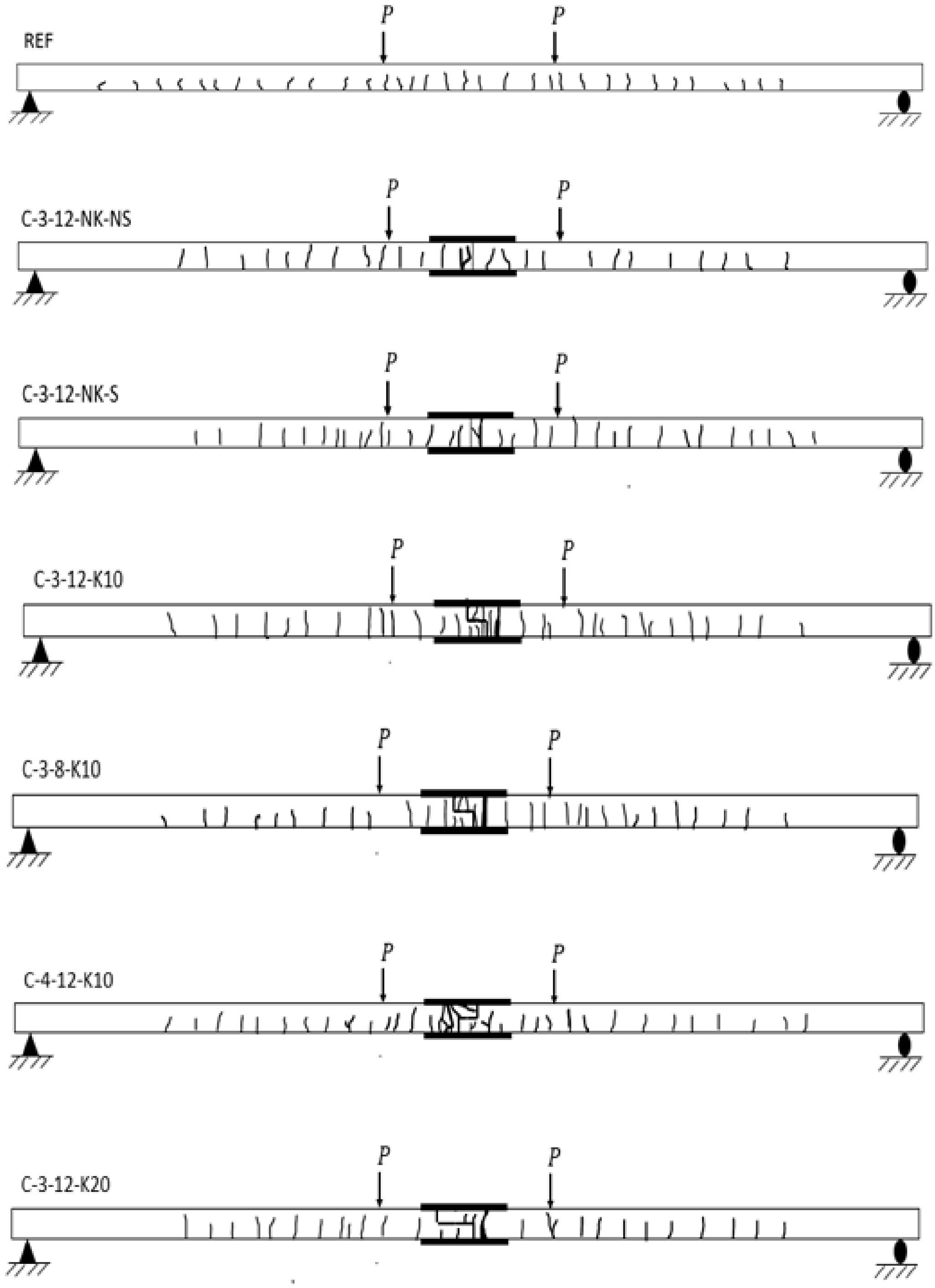

Figure 10: Manually recorded cracks for the slabs tested.

a.REF

b. C-3-12-NK-NS

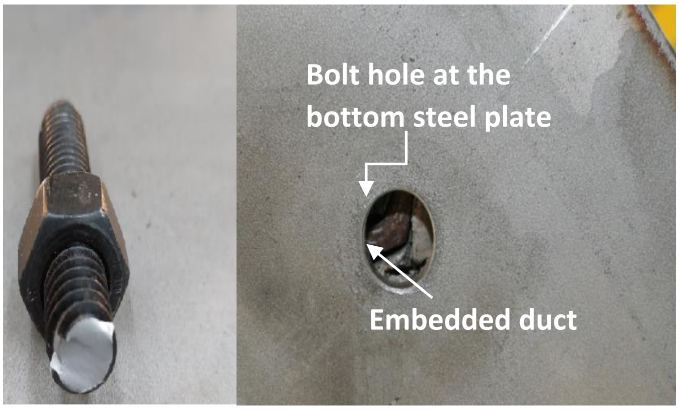

c. C-3-12-NK-S

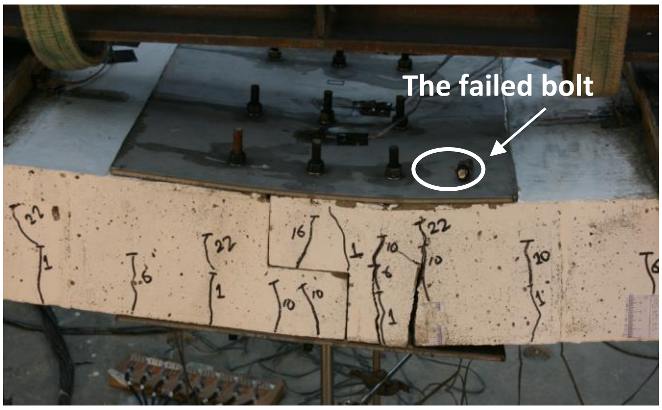

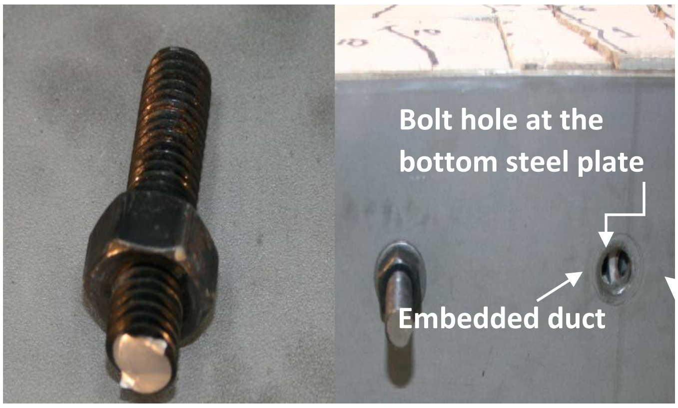

d. C-3-12-NK-S

Figure 11-1: Mode of failure of the slabs tested.

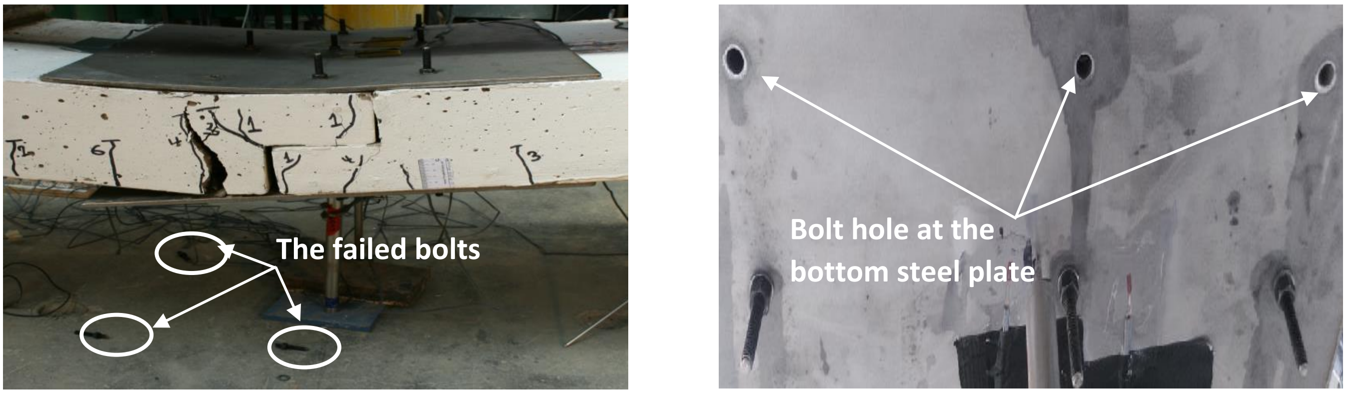

e. C-3-8-K10

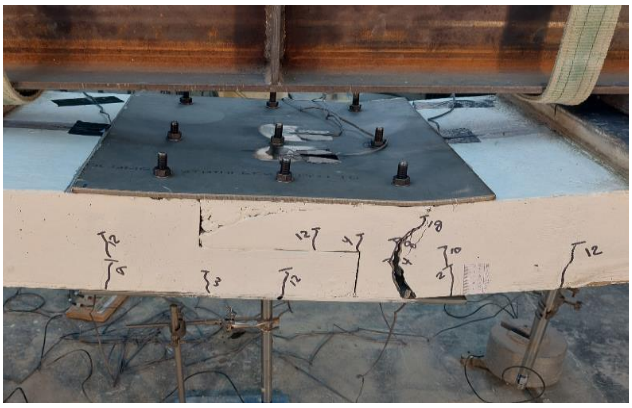

f. C-3-12-K20

g. C-4-12-K10

Figure 11-2: Mode of failure of the slabs tested.

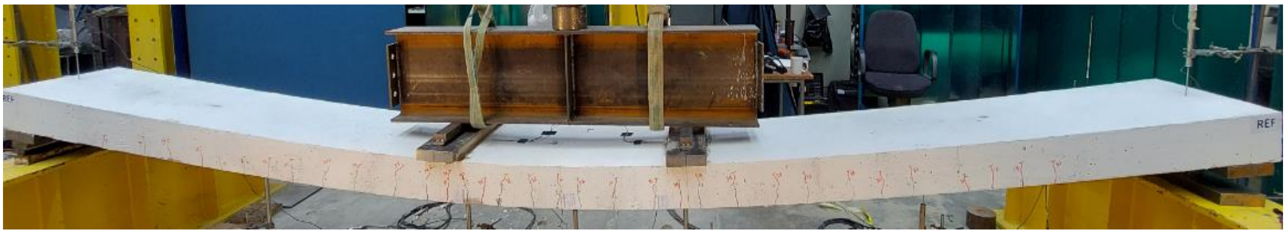

a. Control

b. C-3-12-NK-NS

c. C-3-12-NK-S

d. C-3-12-K10

e. C-3-8-K10

f. C-3-12-K20

g. C-4-16-K-B

Figure 12: The deformation shape of the slabs tested.

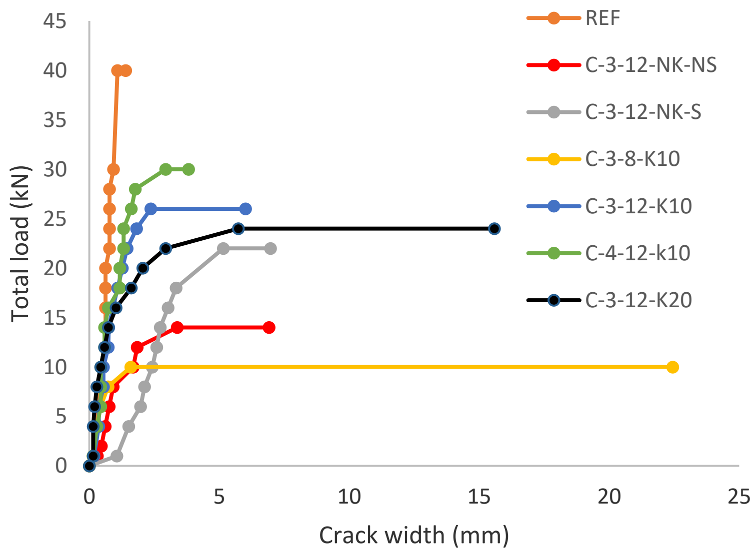

Figure 13: The crack width of dominant crack of the slabs tested at the mid-span section.

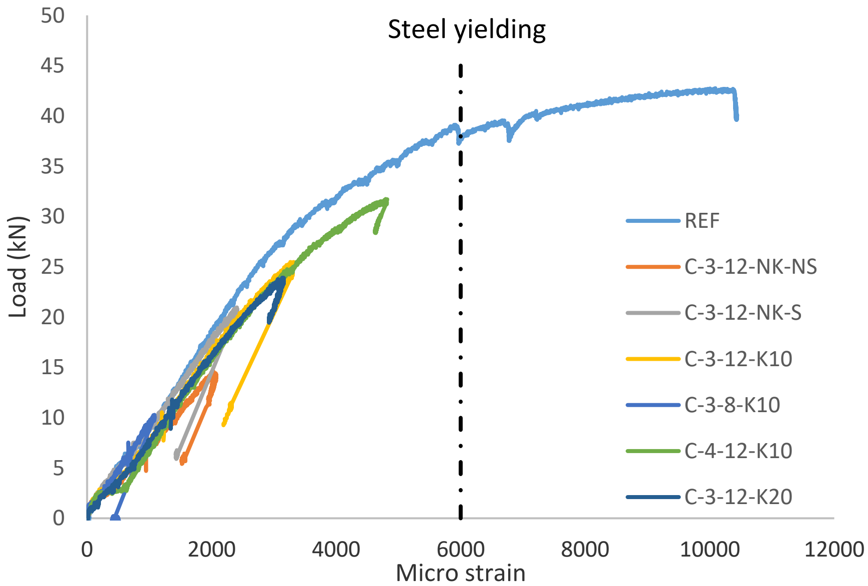

Figure 13: The variation of the stainless steel tensile strain against the total applied load of the tested specimens.

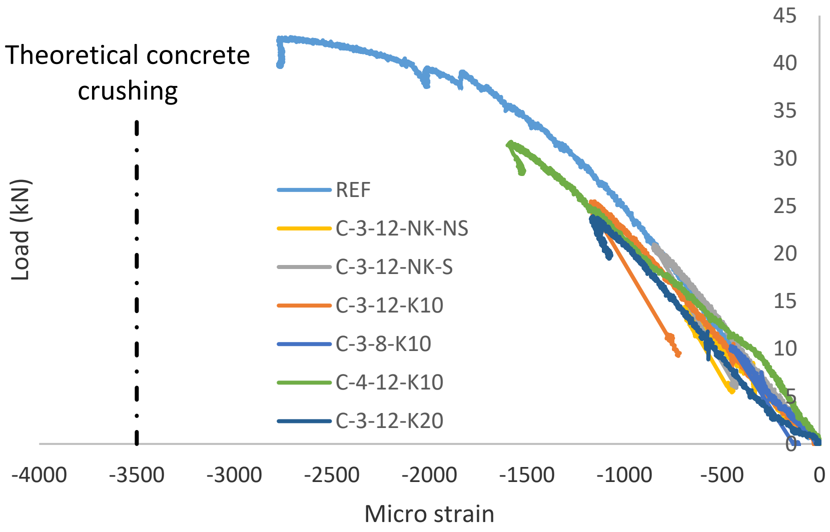

Figure 14: The recoded strain value in concrete at the compression side.

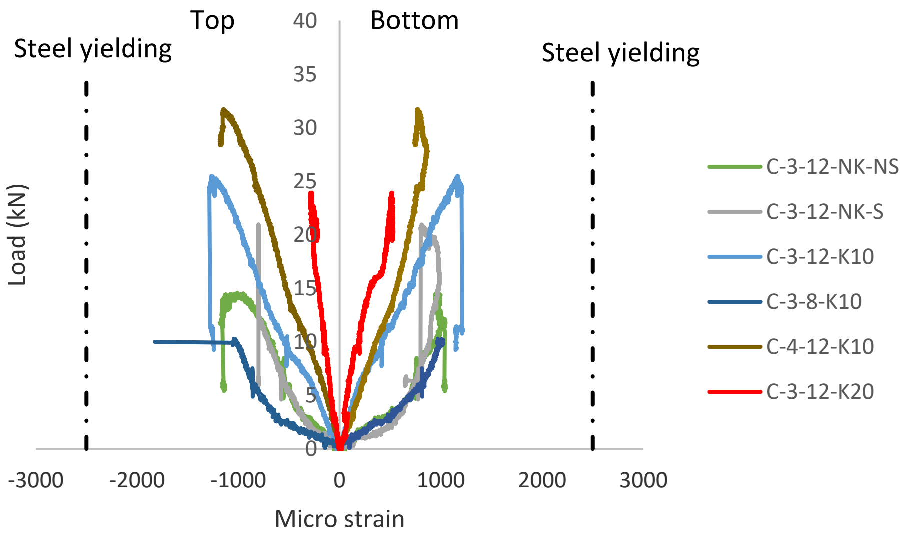

Figure 15: The strain value at the top and bottom steel plate of the documentable slabs.

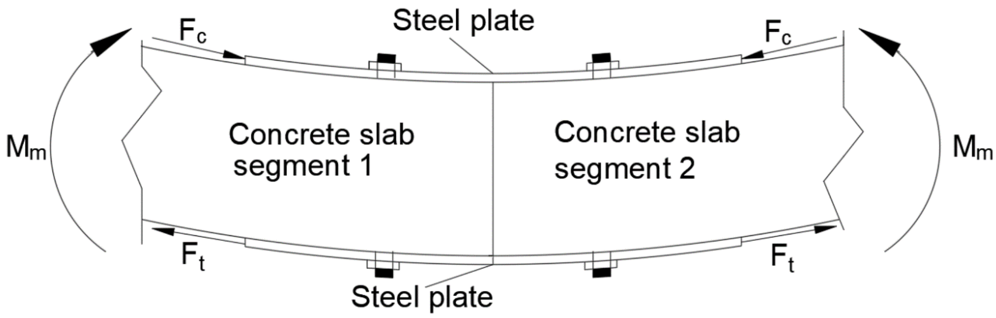

a. Force transfer through steel plates

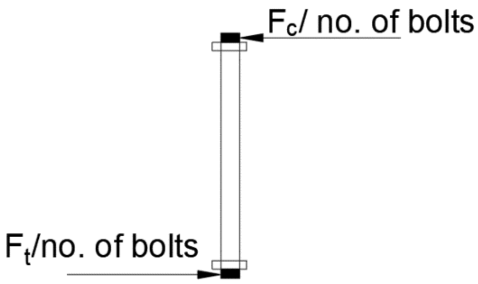

b. Force transfer through steel bolts

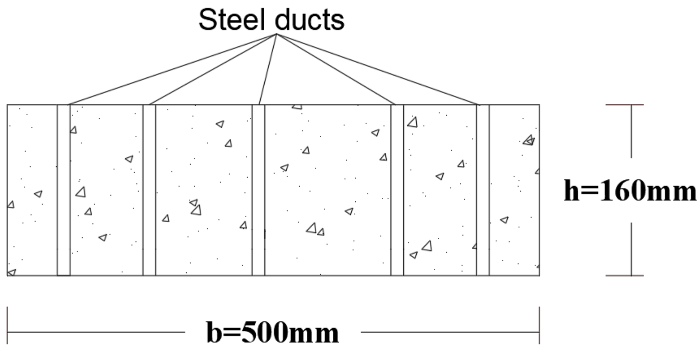

c. Details of net section area of concrete along the bolt.

Figure 17: Forces transformation in demountable slabs.

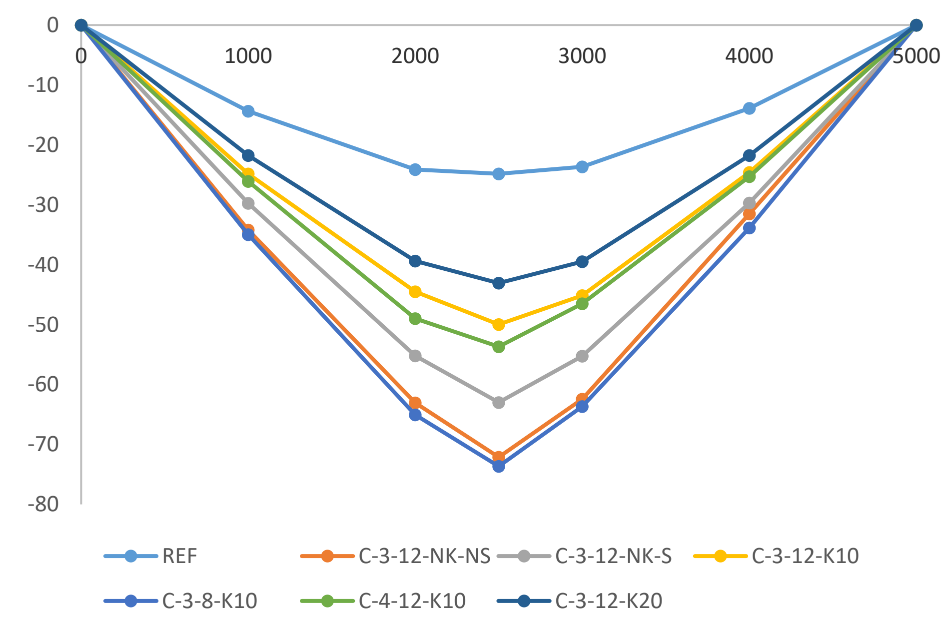

Figure 18: deflection profile for the slabs tested at 10.3 kN.

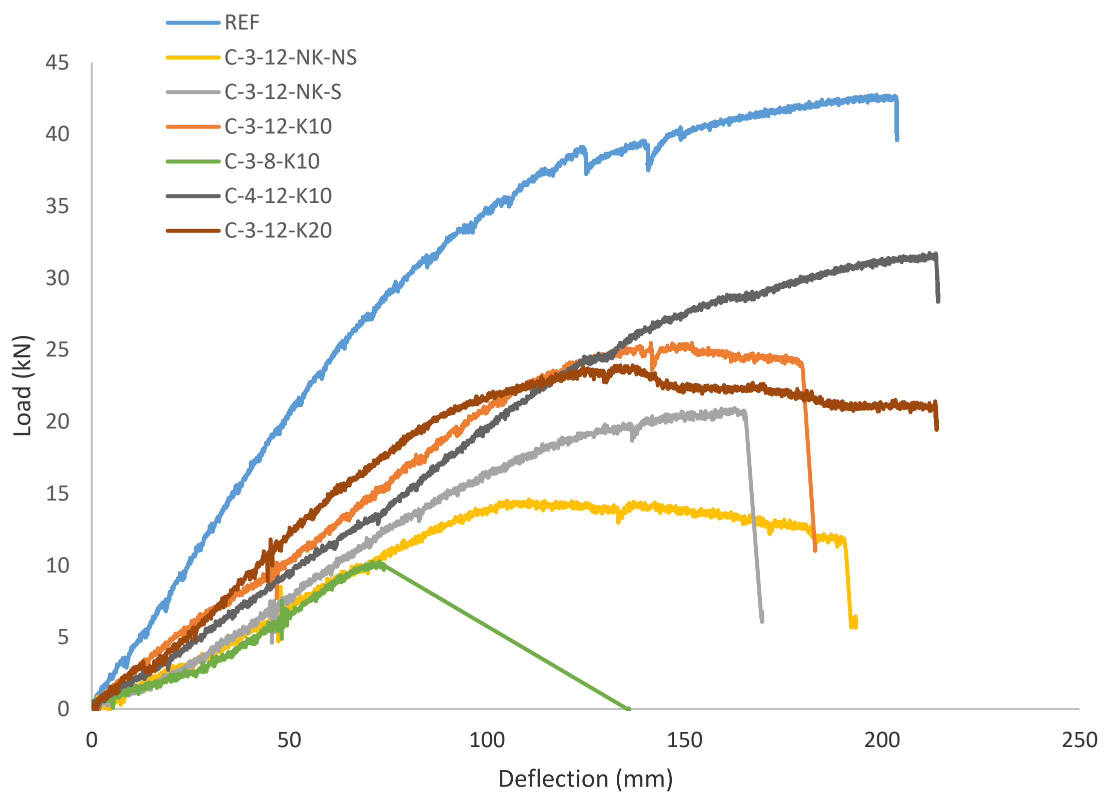

Figure 19: Load-deflection response of the slabs tested.

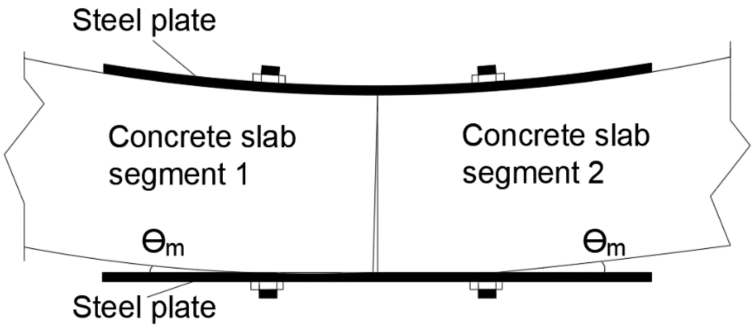

Figure 20: Midspan rotation at the demountable connection.

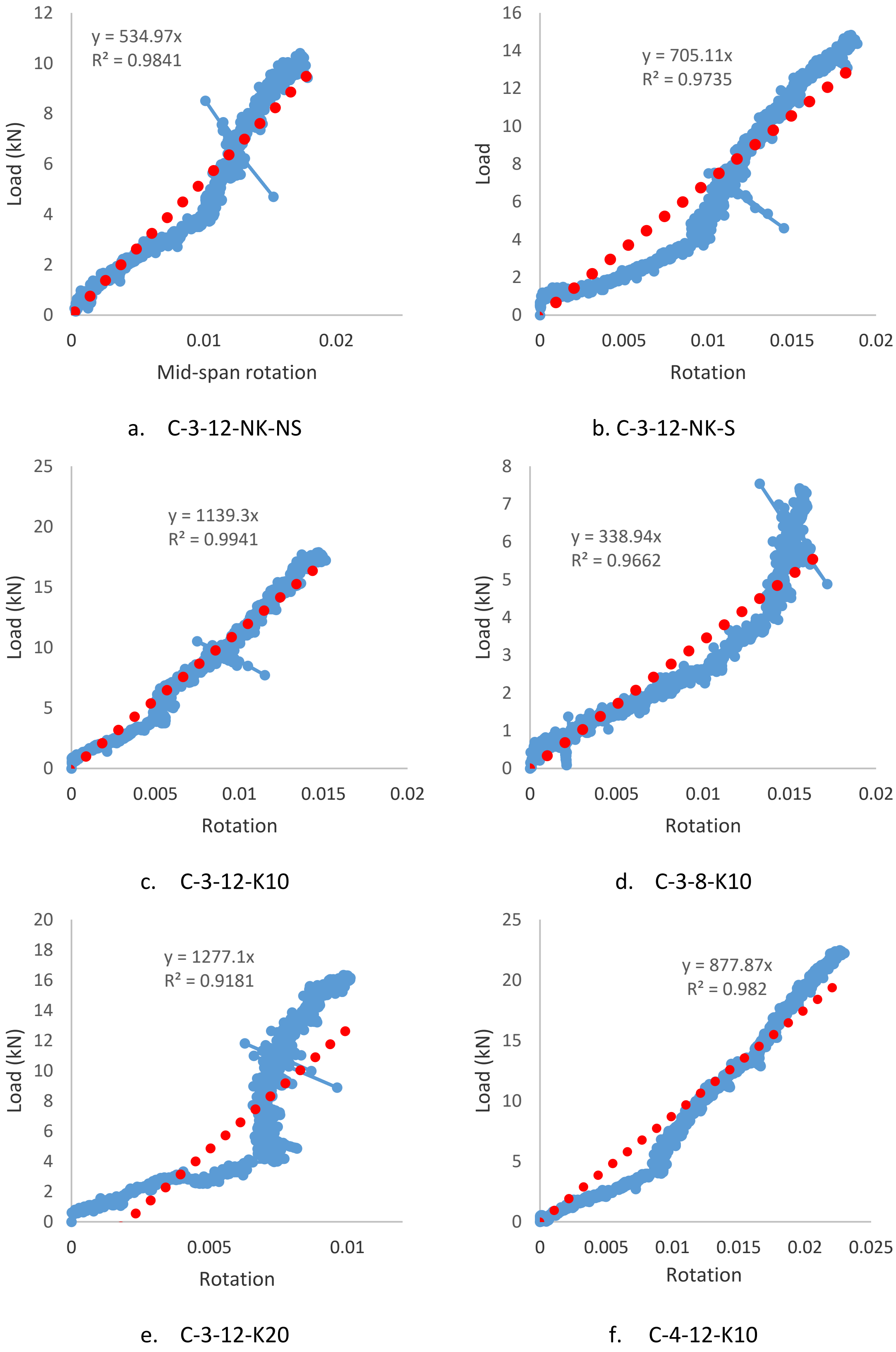

Figure 21: Load-deflection response of the slabs tested.

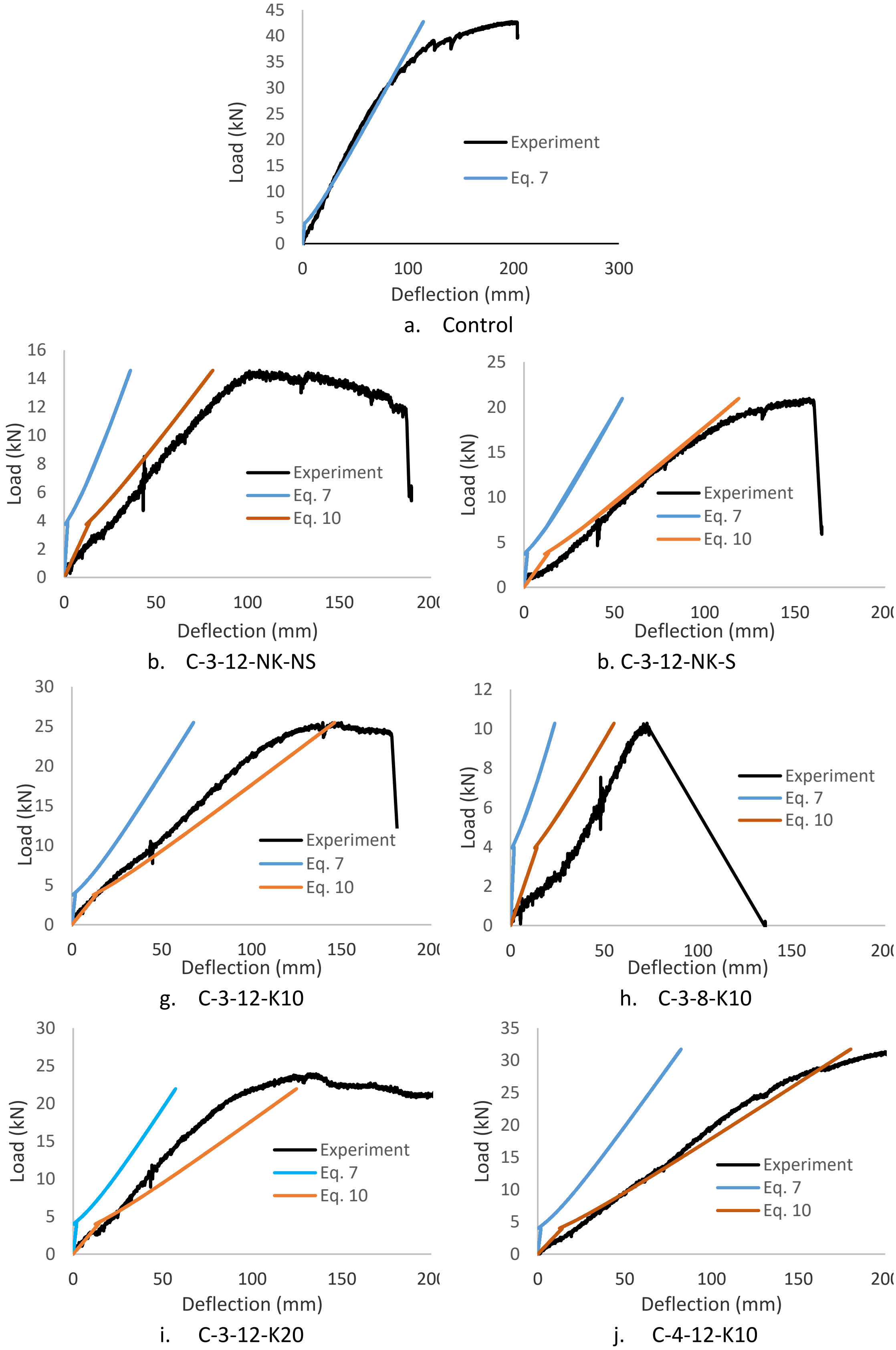

Figure 22: Load-deflection response of the slabs tested.